

Dielectric Ceramic EPR Resonators for Low Temperature Spectroscopy at X-band Frequencies

Stefan Friedländer · Oleg Ovchar · Horst Voigt ·
Rolf Böttcher · Anatolii Belous · Andreas Pöpl

Received: 23 September 2014
© Springer-Verlag Wien 2014

Abstract The performance of new dielectric ceramic resonators (DRs) for continuous wave (cw) X-band electron paramagnetic resonance (EPR) spectroscopy is investigated at room temperature and low temperatures (77, 6 K). The DRs with high dielectric constants of about $\varepsilon_r = 80$, featuring low residual paramagnetic impurities, have been developed and produced on the basis of barium lanthanide titanates solid solutions with the general formula $\text{Ba}_{6-x}\text{Ln}_{8+2x/3}\text{Ti}_{18}\text{O}_{54}$ ($\text{Ln} = \text{Sm}, \text{Nd}$) that demonstrate at once low dielectric losses in the microwave range ($\tan \delta = 7\text{--}14 \times 10^{-4}$ at 10 GHz) and appropriate temperature stability of the dielectric constant ($\tau_\varepsilon = \pm 5$ ppm/K). They were optimized for samples with small dimensions and can be used in commercial Oxford instruments flow cryostats if the coupling is done via cavity resonators. We found a maximal EPR signal enhancement by a factor up to 74 at 6 K. The increases of quality and filling factors as well as that of the microwave (mw) B_1 -field in the resonator setup are discussed in dependence on temperature. We show that the absolute sensitivity gain must be related to that increase in the mw field and the remaining relative gain of the SNR is

Electronic supplementary material The online version of this article (doi:[10.1007/s00723-014-0611-x](https://doi.org/10.1007/s00723-014-0611-x)) contains supplementary material, which is available to authorized users.

S. Friedländer · H. Voigt · R. Böttcher · A. Pöpl (✉)
Institute of Experimental Physics II, Leipzig University, Linnéstrasse 5,
04103 Leipzig, Germany
e-mail: poepl@physik.uni-leipzig.de

S. Friedländer
e-mail: friedlaender@physik.uni-leipzig.de

O. Ovchar · A. Belous
Institute of General and Inorganic Chemistry, NASU,
Academician Palladin Avenue 32-34, 03680 Kiev, Ukraine

A. Belous
e-mail: belous@ionc.kar.net

about 18 for small samples. The developed DRs have shown a good potential in EPR application as reliable and easy-to-use components allowing research of thin films and in particular small crystalline structures.

1 Introduction

The high dielectric constants of $\varepsilon_r \approx 80$ of novel dielectric resonators (DRs) allow their usage in commercial flow cryostats with coupling provided via cavity resonators for electron paramagnetic resonance (EPR). The easy-to-use setup offers the opportunity to measure small single crystals and thin film samples at non-ambient atmospheres and a wide temperature range $6\text{ K} \leq T \leq 300\text{ K}$. The application of DRs in EPR is well known and established. At room temperature DRs proved versatility for various solid-state experiments [1] and aqueous samples in stopped flow experiments [2, 3]. Different shapes and designs for DRs have been proposed. They are treated to great extend in [4–8] and are nowadays available in industry design such as the Bruker ER 4123D and 4118X-MD5 resonators. Some DRs were coupled via antennae [9] while others have integrated them into cavity resonators, such as Mattar and Emwas [10] who report signal-to-noise ratio (SNR) gains of stacked DRs of 24 and Jaworski et al. [1] with SNR gains of more than 30 at room temperature depending on the sample. DR materials that support low temperature measurements were reported to give SNR gains of up to 170 at 77 K in the work of Golovina et al. [11]. Also, ferroelectric materials were proposed due to their high permittivities with SNR enhancements up to 100 [12, 13].

Experiments with DRs at temperatures below 77 K are more challenging regarding custom DR design and material considerations. Appropriate relative dielectric constants ε_r and acceptable dielectric losses $\tan \delta$ with negligible temperature dependencies in a wide temperature range limit the usability of DRs in general and moreover, contaminants from paramagnetic impurities are a big issue. Rutile was reported as suitable material for DRs [14] but it often contains residual impurities. Furthermore, it features substantial temperature dependencies of the stability of ε_r , τ_e and of $\tan \delta$ between 6 and 300 K [15]. A discussion of the DR materials sapphire and rutile as well as perovskite-based ceramics is presented in the work of Golovina et al. [11], where the authors express the need of high dielectric permittivity materials for low cost employability of DRs in existing cryogenic systems. Our goal was to show that DRs provide an easy-to-use setup for commercial spectrometers, where the DR is placed in a typical EPR sample tube together with the studied sample as shown in Fig. 1a to perform experiments under non-ambient gas atmospheres such as in vacuum or under gas loading at temperatures below 77 K. Then the DRs' dimensions are limited by the inner diameters of the sample tube and the cryostat. DRs can be equipped with holes to accommodate samples at more suitable positions regarding SNR enhancements as explained later which is depicted in Fig. 1b.

As shown in Fig. 1c, cylindrically shaped DRs of certain dimensions are assumed to resonate most efficiently in the $\text{TE}_{01\delta}$ -mode following the notation of [16]. To obtain this mode a certain geometry and proper values of ε_r and $\tan \delta$ of the DR

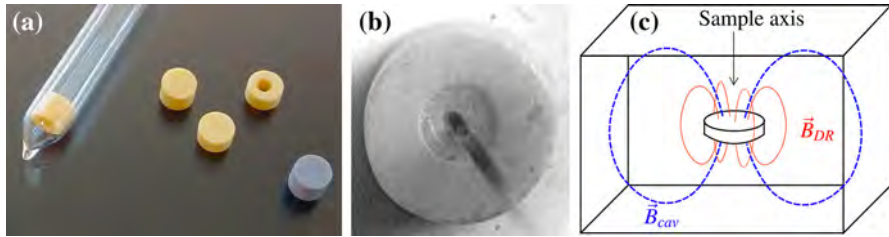


Fig. 1 **a** DRs (from left to right): K80-H in sample tube, K80, K80', K80-H' next to the differently colored K85; their size is given in Table 1. **b** The samples can be inserted in a capillary and positioned inside the DR to achieve the highest SNR gains. Here, a thin capillary ($\phi = 200 \mu\text{m}$) is positioned with grease inside the hole of K80 ($\phi = 1 \text{ mm}$). **c** Superposition of $\text{TE}_{01\delta}$ -mode of a DR (thin, red) and TE_{102} mode of the cavity resonator (dashed, blue) in the notation of [16] (color online)

material at the given temperature are needed. The dielectric properties need to have a sufficiently low temperature dependence to ensure usage in the temperature range $6 \text{ K} \leq T \leq 300 \text{ K}$. The frequency f_{free} that is usually considered as optimal when employed in cavity resonating systems is close to the frequency of that very metal cavity resonator [11]. In the work of D. Kajfez [17] an approximate equation of the frequency of the $\text{TE}_{01\delta}$ -mode is given as

$$f_{\text{GHz}} = \frac{34}{a\sqrt{\epsilon_r}} \left(\frac{a}{L} + 3.45 \right) \quad (1)$$

where the radius of the DR is denoted by a and its height by L (both measured in units of mm). This formula gives a good approximation if the ratio a/L of cylindrically shaped DRs and its permittivity meet the following requirements:

$$0.5 < \frac{a}{L} < 2 \quad \text{and} \quad 30 < \epsilon_r < 50. \quad (2)$$

A more accurate empirical formula has been derived from simulations by Kishk et al. [16]:

$$f_{\text{GHz}} = \frac{2.921c\epsilon_r^{-0.465}}{2\pi a \cdot 10^6} \cdot \left[0.691 + 0.319 \frac{a}{L} - 0.035 \left(\frac{a}{L} \right)^2 \right] \quad (3)$$

where c is the speed of light in vacuum. Kishk et al. [16] show that for arbitrary ϵ_r individual simulations would be necessary and if the ratio of a/L is out of the range as specified in (2), other modes may be enhanced while the mode of avail can be suppressed. In our measurements the DRs have to be suited for X-band frequencies between 9 and 10 GHz. The Oxford ESR 900 flow cryostat supports cylindrical sample tubes of up to 5 mm outer diameter [18]. Therefore, we chose the DRs' outer diameter to be less than 4 mm which enables the employment of quartz glass sample tubes with 500 μm wall thicknesses to accommodate the DR together with the sample in the test tube at non-ambient atmospheres. According to Eqs. 1–3 this geometry requires relative permittivities of the DRs of 70 or more to serve for X-band frequencies. More sophisticated ways of predicting required dimensions employing finite element simulation or novel improvements of coupled mode theory (CMT) are presented by other authors [19–21]. Those theoretical investigations with

simulations and CMT of DRs coupled to cavity resonators found the $TE_{01\delta}$ mode being able to couple in a parallel (symmetric, in phase) and antiparallel (antisymmetric, out of phase) configuration with respect to the TE_{102} or TM_{110} modes of the rectangular or cylindrical cavities, respectively [7, 11, 19–21]. The parallel field superposition results in lower resonance frequencies and the antiparallel fields shows the opposite behavior with higher coupled microwave (mw) resonance frequencies. Higher frequencies yield lower signal enhancements, while the lower frequencies are the preferred ones with even higher SNR gains. The low frequency parallel mode was experimentally excited for DRs with lower $\varepsilon_r \approx 35$ [11] whereas the high frequency antiparallel mode is reported to be the dominating one for DRs with higher ε_r . Mett et al. [19] state that with an iris coupling of electrically coupled cavity-DR systems only one of such modes can be excited at the same time and the coupled resonance frequencies with $f_{\text{antiparallel}} > f_{\text{empty cav.}} > f_{\text{parallel}}$ never cross.

One more difficulty arises when comparing the SNR gains from the publications stated above. It is important to notice, that all experiments which compare the SNR have to be carried out at the same measurement conditions. This, however, results in the situation that the augmented mw B_1 -field is not considered in many of the publications besides [5] and [22]. In our approach, the B_1 -field will be taken into account and the SNR gains can be considered as purely due to the change in the quality factor Q and the filling factor η , yet not due to the increase in the incident mw power P as this can be chosen to be sufficiently high in most cw EPR experiments in principle. Hence, the SNR can be found from the absorption signal intensity χ'' according to [23] as

$$\text{SNR} = \frac{\langle P_{\text{signal}} \rangle}{\langle P_{\text{noise}} \rangle} \propto \frac{\eta Q \chi''(T, I) \sqrt{P}}{\sqrt{k_B T \Delta f}} \quad (4)$$

with T being the temperature and $\sqrt{k_B T \Delta f}$ the expression for the thermal noise with Δf being the amplifier bandwidth. For all measurements, the increase in SNR is denoted as ‘SNR gain’ containing both the increase in mw field power P and the ‘relative gain’ due to changes in η and Q , with η being itself dependent on the mw magnetic field distribution in the vicinity of the sample [23]:

$$\eta = \frac{\int_{\text{sample}} B_1^2 dV}{\int_{\text{resonator}} B_1^2 dV}. \quad (5)$$

A proportionality constant C for the incident mw power to B_1 -field conversion which is referred to as probe’s efficiency parameter 2Λ by other authors [19, 20] can be given as

$$B_{1,i} = C_i \sqrt{P} = 2\Lambda \sqrt{P}. \quad (6)$$

We will stick to the proportionality definition mostly throughout this paper for convenience as we only give relative numbers. To test the relative conversion factors C_i/C_{ref} of all DR_i resonators coupled to the resonator–cryostat combination of the Bruker ER 4105DR equipped with the Oxford ESR 900 versus this resonator–cryostat combination serving as reference with conversion factor C_{ref} , a

homogeneously saturating sample can be used [23]. An accurate procedure is shown by Nesmelov et al. [22], who relate the rollover saturation curves to the square root incident mw power. Here, the resonators are compared by the point with half rollover saturation. The method is particularly advantageous for small saturation powers since it does not rely on identifying a maximum in a saturation curve at powers as low as a few hundred nanowatts (nW). With the help of this information the sensitivity enhancement due to a change in η and Q can be separated from the signal enhancement due to the increasing mw power. An increase of the SNR by a factor n can also be achieved by accumulating n^2 -times since the noise figure is reduced by the square root of scans [23]. Therefore, an equivalent number of scans will be applied in Sect. 3.3 in our experiment for comparing the SNR at different powers.

2 Experimental Methods

2.1 DR Material

The resonators shown in Fig. 1 were made of oxide ceramics with the composition $\text{Ba}_{6-x}\text{Ln}_{8+2x/3}\text{Ti}_{18}\text{O}_{54}$ ($\text{Ln} = \text{Sm}, \text{Nd}$) that belong to a wider family of barium lanthanide titanates (BLTss) with the structure of tetragonal tungsten bronze (TTB). The basic compositions of the ceramics have been slightly modified by means of partial iso- and aliovalent substitution in their crystalline lattices to suppress mw dielectric loss and improve temperature stability of the dielectric constant

$$\tau_\varepsilon = \frac{1}{\varepsilon} \frac{\partial \varepsilon}{\partial T}. \quad (7)$$

The latter parameter is crucial in terms of suppressing the temperature changes of the resonant frequency of a DR. In this regard, the DRs' materials generally contain also slight amounts (up to 1–5 % wt.) of calcium, strontium, and magnesium oxides. The ceramics were made by solid-state synthesis at a sintering temperature of 1,350 °C for 6–8 h. A cylindrical compression mold of the necessary diameter was used [24]. Further machining was done by grinding off parts of the cylinder height L to match the coupled DR-cavity frequency to the cavity resonators equipped with the flow cryostat. Here, the coupled frequency was chosen such that it falls in the range of 9.10–9.90 GHz accessible by our spectrometer regarding the changing DR frequency when the DR is confined by the walls of the resonator. Some DRs are equipped with a 1 mm hole for sample insertion as shown in Fig. 1. The dielectric constant of the resonators has been adopted to values around $\varepsilon_r = 75$ –85 to meet the geometrical requirements explained above (see Sect. 1). As a consequence, the DRs demonstrated low dielectric losses in the microwave range ($\tan \delta$ below 10^{-3} at 10 GHz), and good temperature stability of the dielectric constant ($\tau_\varepsilon = \pm 5$ ppm/K). Two sets of DRs having $\varepsilon_r = 80$ and $\varepsilon_r = 85$ labeled K80 and K85, respectively, have been selected for application in EPR spectroscopy. The dimensions and the frequencies of the unmatched DRs and coupled DR-cavity systems are given in Table 1.

Table 1 Geometrical and mw parameters of unmatched DRs and DRs coupled to a resonator–cryostat combination with a Bruker ER 4105DR and an Oxford ESR 900

DR	T (K)	ε_r	Shape	$2a$ (mm)	L (mm)	f_{free} (GHz)	f_{coupled} (GHz)	Q	VSWR
ER-4105DR	300		Empty cavity				9.62	$3,400 \pm 50$	1.005
	77							$3,400 \pm 50$	1.01
	6							$3,400 \pm 50$	1.03
K80	300	80	Disk	3.4	2.9	9.05	9.73	$2,300 \pm 50$	1.025
	77							$2,400 \pm 50$	1.035
	6							$2,400 \pm 50$	1.060
K80'	300				2.0	9.72	9.90	$1,600 \pm 100$	1.05
	77							$1,800 \pm 100$	1.08
	6							$1,600 \pm 100$	1.06
K80-H	300	80	Ring	3.5	2.8	9.12	9.75	$2,500 \pm 100$	1.095
	77							$2,800 \pm 100$	1.100
	6							$2,500 \pm 100$	1.160
K80-H'	300				2.0	9.74	9.89	$1,500 \pm 100$	1.61
	77							$2,000 \pm 100$	1.25
	6							$2,100 \pm 100$	1.27
K85	300	85	Disk	3.4	2.8	9.14	9.86	$2,300 \pm 50$	1.025
K85'	300							$1,600 \pm 100$	1.05

The error in the lengths is less than 0.05 mm, f does not differ more than 5 MHz at the different temperatures

2.2 DR Microwave-Network Coupling

The unmatched frequency f_{free} of the $\text{TE}_{01\delta}$ -mode weakly coupled to an antenna has been measured in a cylindrical shield of sub-wavelength dimensions with an HP/Agilent Technologies 8510C network analyzer system equipped with a HP 8514B S -parameter test set. For later EPR experiments the coupling of the DRs to the mw network was achieved by insertion of the DRs into the resonator–cryostat combination with a Bruker ER 4105DR rectangular resonator and an Oxford ESR 900 cryostat. The DRs were placed at the lower end of a standard EPR quartz-glass sample tube with an inner diameter of 4 mm. The frequencies f_{coupled} of the coupled DRs and quality factors Q in Table 1 were acquired using the network analyzer at the regular EPR setup, replacing the usual mw bridge. Usual values for the voltage standing wave ratio (VSWR) of the coupled DRs in the cavity are between 1.05 and 1.3 and hence close to, but larger than those of empty cavity resonators. Therefore, coupling can be limited down to only three to four orders of magnitude of power at very low temperatures. The S_{11} -parameter return loss in logarithmic units at critical coupling is typically around -45 dB while an empty cavity resonator can have values of about -60 dB. The quality factor was determined according to the 3 dB

method for the bandwidth Δf with $Q = f_{\text{coupled}}/\Delta f_{\text{coupled}}$ [23] and recorded at the coupled frequency, which was obtained for the DR being centered in the vertical sample axis of the cavity resonator. At this position, the antiparallely coupled mode has the lowest frequency. The measured overall quality factor Q of the coupled cavity-DR system is always lower than the quality factor of the resonator-cryostat combination. This is in accordance to theoretical predictions for coupled DR-cavity systems, that relate the probe's efficiency parameter Λ as inversely related to the quality factor [19]. The tolerance in Q is mostly due to the difficulty to separate the DR mode from reflections in the microwave network. The Online Resource for this paper shows all modes of shielded DRs coupled via antennae and the identification of the cavity-coupled mode as $\text{TE}_{01\delta}$ -mode.

2.3 EPR Measurements and Test Samples

The EPR measurements were carried out using a Bruker EMXmicro X-band spectrometer equipped with a Bruker ER 4105DR double cavity resonator and an Oxford ESR 900 flow cryostat for low temperature measurements (the –DR stands for ‘double cavity’ and should not be confused with the notation used elsewhere in this paper). The usage of a double cavity resonator allows parallel measurements of reference samples to compare the quality factor at a series of quantitative measurements. We consider the Bruker ER 4105DR double cavity resonator as a likely setup for quantitative low temperature measurements and compare the DRs with respect to and in that cavity resonator.

To test the relative conversion factors C_i/C_{ref} , a homogeneously saturating sample of 1,3-bisdiphenylene-2-phenylallyl (BDPA) was used. C_{ref} is obtained from the resonator-cryostat combination without DR for all sensitivity enhancements stated in Tables 2, 3 and 4 and is taken into account for all SNR enhancements given in this publication. Moreover, special care has to be taken to avoid saturation of the SNR test samples used to compare the signal intensities. Therefore, all measurements have to be carried out at sufficiently small mw powers which result in a linear relation between the EPR signal intensity and the B_1 -mw field. To avoid saturation effects on the test samples described above smallest powers between 200 and 800 nW were frequently used for all measurements. Settings as the receiver

Table 2 C_i/C_{ref} and SNR gains of the different DRs and the resonator-cryostat combination at room temperature

Resonator	C_i/C_{ref}	SNR gain	Normalized gain
4105DR	1	1	1
K80	1.4 ± 0.2	2.2 ± 0.4	1.6 ± 0.4
K80'	2.0 ± 0.2	8.0 ± 0.4	4.0 ± 0.4
K85	1.5 ± 0.2	2.8 ± 0.5	1.9 ± 0.5
K85'	2.1 ± 0.2	8.2 ± 0.5	3.9 ± 0.5
K80-H	3.6 ± 0.4	40 ± 3	12 ± 2
K80-H'	4.2 ± 0.5	80 ± 3	19 ± 3

Table 3 C_i/C_{ref} and SNR gains of the different DRs and the resonator–cryostat combination at 77 K

Resonator	C_i/C_{ref}	SNR gain	Normalized gain
4105DR	1	1	1
K80	1.5 ± 0.3	3.0 ± 0.2	1.5 ± 0.3
K80'	2.8 ± 0.3	13.5 ± 0.5	4.8 ± 0.4
K80-H	3.8 ± 0.4	38 ± 2	10 ± 2
K80-H'	4.3 ± 0.5	78 ± 3	18 ± 3

Table 4 C_i/C_{ref} and SNR gains of the different DRs and the resonator–cryostat combination at 6 K

Resonator	C_i/C_{ref}	SNR gain	Normalized gain
4105DR	1	1	1
K80	1.6 ± 0.3	1.8 ± 0.2	1.1 ± 0.3
K80'	1.9 ± 0.3	6.2 ± 0.5	3.3 ± 0.4
K80-H	4.2 ± 0.5	36 ± 2	8.5 ± 2
K80-H'	4.8 ± 0.6	74 ± 3	15 ± 2

gain, modulation amplitude (0.3 mT) and -frequency (100 kHz) were left constant during all SNR measurements.

The test sample used for the SNR measurements was a MgO:Cr^{3+} powder sample with magnetically diluted paramagnetic Cr^{3+} ions due to good scalability and signal reproducibility. Also, transition metal ions are proper candidates for possible future use of the DRs in application of chemical research. Here, the Cr^{3+} transition metal ion has an electron spin of $S = \frac{3}{2}$ but it is incorporated in the cubic Mg sites in the MgO structure leading to a vanishing zero field splitting. Therefore, only a single EPR line is observed [25]. The ^{53}Cr hyperfine (hf) interaction ($I_{53\text{Cr}} = \frac{3}{2}$) signals have not been examined because of the low natural abundance (9.5 %) of that isotope. The sample volume was fixed and sealed in small quartz glass mark tubes of 200 μm inner diameter leading to a sample volume of about 20 nl. The mark tube fits in all ring DR (inner diameter of 1 mm) and can be centered in the middle of the DR for example with grease as shown in Fig. 1b. The MgO:Cr^{3+} sample was kept small in size as it was proposed that smaller samples give higher SNR gains [11]. For the other, disk-shaped DRs the same sample was put on top of the disk DR to mimic future thin film applications. Here, not all of the samples can be perfectly centered and the sample size and volume is a compromise between number of spins (as much as possible) and sample volume (as small as possible). The same sample of MgO:Cr^{3+} was used for all comparison measurements with a SNR of several thousands at 6 K in the ring DRs but merely 10–300 K without DR, which determines the error in the SNR measurements. All spectra of the MgO:Cr^{3+} sample were recorded in a single scan with a mw power of 60 μW , a modulation amplitude of 0.3 mT and a conversion time of 10 ms. The obtained Cr^{3+} EPR absorption signals have been double integrated for comparison. Then, the

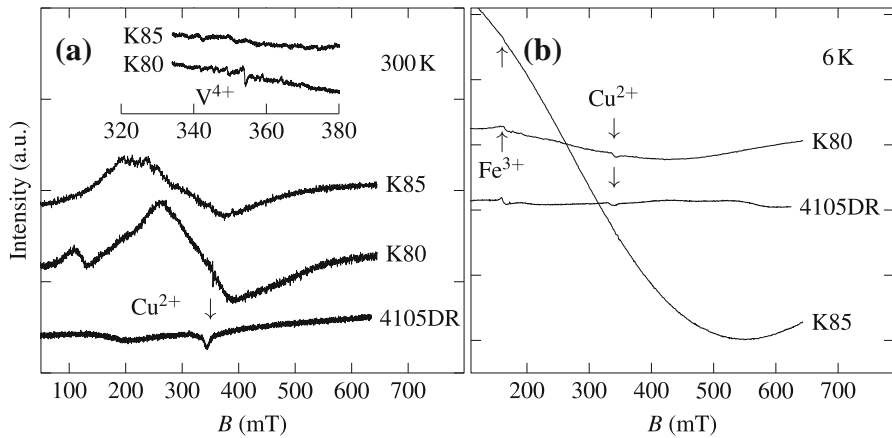


Fig. 2 X-band EPR spectra of K80 and K85 DRs as seen in the plots for **a** room temperature (10 scans) including an *inset* showing more details around $g = 2$ and **b** 6 K sample temperature. The arrows $\uparrow\downarrow$ in the low temperature plot **b** indicate impurity signals from the resonator-cryostat combination and are, therefore, good reference signals

SNR gain was determined by comparing the double integral figures within one temperature under the assumption of constant noise levels independent from the used resonator.

In addition a $10 \times 10 \times 100 \mu\text{m}^3$ single crystal of the $\text{Cu-MOF}_\infty^3 [\{\text{Cu}_2^{\text{I}}\text{Cu}_2^{\text{II}}((\text{Me-trz-mba})_2\text{thio})(\text{H}_2\text{O})_2\}\text{Cl}_2] \cdot 6\text{H}_2\text{O}$ initially synthesized by P. Eckhold similarly as reported in [26] was used to demonstrate the applicability for current porous material research. The crystal contains two magnetically inequivalent Cu^{2+} sites ($S = \frac{1}{2}$) which exhibit EPR spectra with resolved ^{63}Cu hf splitting into four lines.

3 Results and Discussion

3.1 Background Signal

To obtain the desired mw characteristics the ceramics for DRs is doped by a number of transition metal ions and rare earth elements, some of them may give rise to paramagnetic impurities. EPR spectra of those impurities must not interfere with the studied EPR signals in a broad temperature range. Therefore, EPR characterization of the used DR materials is necessary. Spectra for the DR materials originating from typically sized DRs are given in Fig. 2. At room temperature, K85 reveals almost no paramagnetic signals (Fig. 2a). A weak signal with a large peak-to-peak line width of $\Delta B_{\text{pp}} = 200 \text{ mT}$ of unknown origin can be subtracted from spectra as baseline correction. As seen from the inset in Fig. 2a some very weak remaining signals around $g \approx 2.0$ with a SNR of 1 or less are visible after 10 scans which cannot be attributed to any impurity directly. Furthermore, a small signal at $g = 2.92$ is

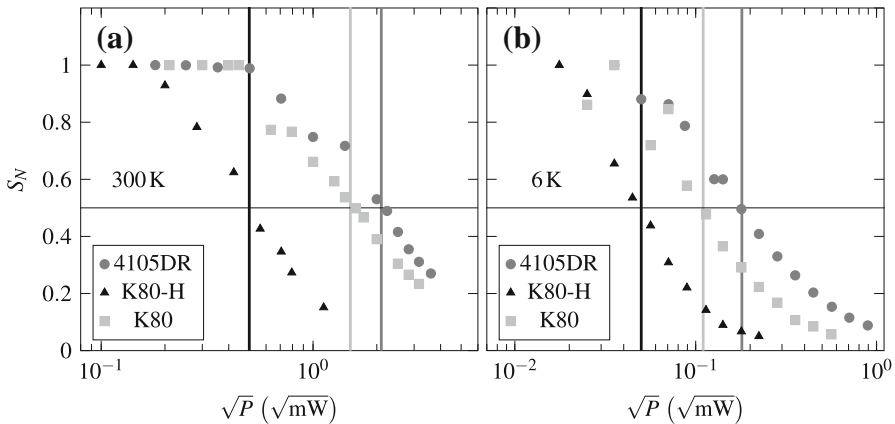


Fig. 3 Rollover saturation curve of BDPA at **a** 300 K and **b** 6 K of the coupled DRs K80, K80-H and the resonator–cryostat combination. \sqrt{P} denotes the root of the incident mw power and $S_N = (S(P)/\sqrt{P})/(S(P')/\sqrt{P'})$ with a reference value $S(P')$ from a non-saturating low power P' . The horizontal line marks the half saturation rollover signal, the vertical ones the corresponding half saturation mw powers for each of the three resonators. Their ratios define the relative conversion factors C_i/C_{ref}

visible; its intensity is comparable to that of the impurities in the cryostat as observed for the Bruker ER 4105DR cavity resonator fixed to the Oxford ESR 900 cryostat and, therefore, acceptable. However, at 6 K K85 has a very strong signal with $B_{\text{pp}} = 480$ mT which is much more pronounced.

In contrast to K85, at room temperature K80 has some more of the broad signals and they are more intense than those of K85, among them the largest at $g = 2.4$ with $\Delta B_{\text{pp}} = 170$ mT. In addition, a weak signal at $g = 1.995$ could be attributed to V^{4+} as seen from the 8 line hyperfine pattern due to the $I = \frac{7}{2}$ nuclear spin of ^{59}V ($3d^1$, $S = 1/2$) [27] with an approximate SNR of 1 after 10 scans (inset in Fig. 2a). At 6 K the spectra of K80 reveals a weak and broad signal of unknown origin with a g value of 3.1 and a peak-to-peak line width of $B_{\text{pp}} = 330$ mT. Overall, the signal intensity of the signal in K80 is comparable to that from the Fe^{3+} -impurity in the cryostat as seen in Fig. 2b. The impurity signals at room temperature from K80 may possibly interfere with EPR spectra of interest at room temperature and hence K85 was considered to be better suited for room temperature measurements, whereas K80 DRs were selected for sensitivity enhancement investigations at low temperatures. The ring-shaped DRs reveal no difference in the spectra (not shown).

3.2 B_1 -Field Conversion

Relative microwave (mw) conversion factors C_i/C_{ref} of the coupled DR systems in comparison to the resonator–cryostat combination have been determined by saturation experiments. Figure 3a shows the rollover saturation curves of the two coupled DRs, K80 and K80-H, together with the resonator–cryostat combination at room temperature, where the normalized saturation powers per square root of the

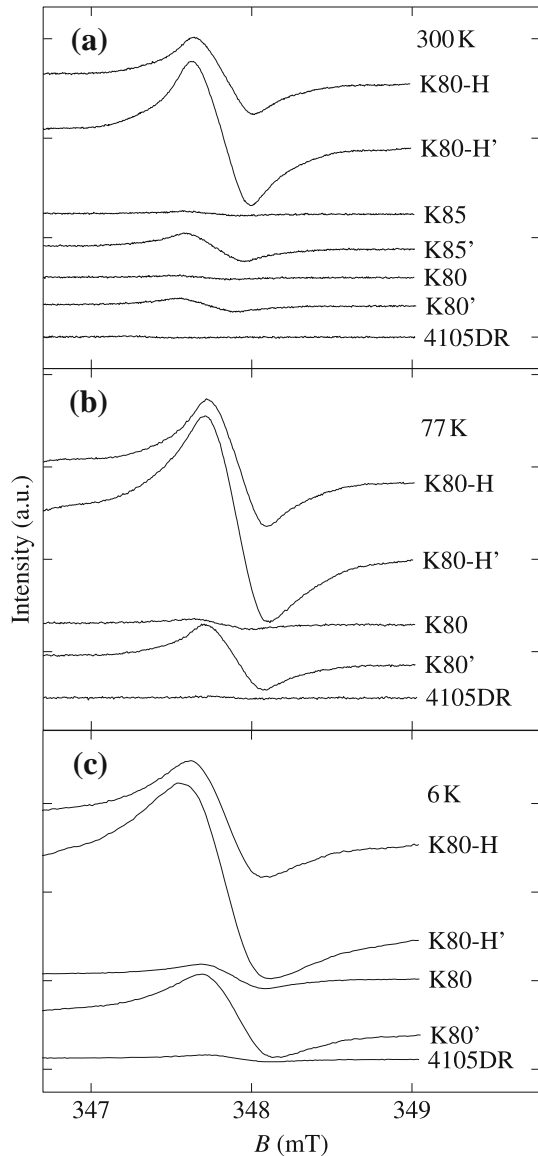
incident mw power of BDPA are plotted versus the square root of the incident mw power [22]. The DRs convert the mw power into stronger B_1 -fields than the resonator–cryostat combination alone. The BDPA sample saturates at about 1.4 times smaller mw powers if placed on top of the DR K80 and at approximately 3.6 times smaller powers in K80-H than for the resonator–cryostat combination without DR. The C_i/C_{ref} are obtained by comparing the half saturation drop square root power values. They are given in the second column of Table 2. A similar behavior is found for low temperatures. The second column in Tables 3 and 4 give the C_i/C_{ref} values for 77 K (without corresponding rollover saturation curves) and 6 K (plot in Fig. 3b).

In general, the DR behavior is similar at all temperatures, that means the order of B_1 -field enhancement is the same within the assumed errors. Among all DRs K80-H' was the DR which enhances the B_1 -field most. It can be seen that smaller L lead to higher frequencies as expected from Eq. 1 and also higher C_i/C_{ref} . Those with higher ε_r and comparable geometry enhance the field a little bit more, while a hole enhances the field significantly more because of the more suitable position of the sample. Theory for the latter observations is covered by other authors already [7]. Special care has to be taken to position the sample right in the middle of the disk. The relative stability of the C_i/C_{ref} as well as f_{coupled} and Q at all measured temperatures supports the small temperature dependences of the dielectric constant and loss tangents reported for the DR material as well as the measured, relatively constant Q -values in Table 1 [24]. All figures for the SNR enhancements are not normalized with respect to C_i/C_{ref} .

3.3 EPR Performance of DRs at Room and Low Temperatures

At room temperature, the performance of the coupled DRs in the resonator–cryostat combination was tested with the MgO:Cr^{3+} sample. The signal enhancement for all investigated DRs is depicted in Fig. 4a. The SNR enhancements achieved in measurements for all tested resonators are given in Table 2. K80 performs worst and has an absolute enhancement of 2.2, related by C_i/C_{ref} this corresponds to a normalized gain in the SNR of only 1.6. The thinner DRs K80' and K85' have a higher enhancement in general by a factor of 1.6–3. The DRs with higher ε_r (K85) have only a slightly higher gain in SNR which is not significant regarding the errors. Still, due to the lower background signal at room temperature, the K85 series was considered as better suited for room temperature measurements. It must be assumed that the actual SNR gain for larger samples can be less if their size extends from the center of the disk-shaped DRs such as thin films. The ring DRs K80-H and K80-H' perform significantly better, if the sample is placed well centered inside the hole. This observation has been stated by several authors before [1, 6, 17]. The absolute SNR enhancement for the highest gain of K80-H' corresponds to a factor of 80 compared to the resonator–cryostat combination without additional DR and is the highest achieved factor at room temperature as well as the relative SNR enhancement of 19 which is the highest increase in SNR that was achieved with the resonators at room temperature.

Fig. 4 EPR spectra of $\text{MgO}:\text{Cr}^{3+}$ at 60 μW mw power at **a** room temperature, **b** at 77 K and **c** at 6 K sample temperature. The *bottom* spectrum in each plot represents the sample in the resonator–cryostat combination, above them with the different DRs to scale within one temperature. All values are given in Tables 2, 3, 4



The DRs K80 and K80-H were also investigated at 77 and 6 K with the $\text{MgO}:\text{Cr}^{3+}$ powder sample while K85 is not suited for these measurements due to the background signal at low temperatures mentioned in Sect. 3.1. Figure 4b, c show spectra of the $\text{MgO}:\text{Cr}^{3+}$ sample at 77 and 6 K, respectively, for the appropriate DRs in comparison to the cavity resonator. The results are given in Tables 3 and 4. The observed signals are, for the marginal enhancements of the disk-shaped DRs, partly more pronounced than at room temperature in accordance to the slightly enhanced Q -values in Table 1. The better defined field distributions in

the ring DRs show a constant behavior within the error ranges. Again, the DRs with smaller L perform somewhat better in general. The highest SNR gains are likewise obtained for K80-H' as in the room temperature experiments. Overall, room and low temperature experiments lead to comparable results.

We confirmed that DRs enhance the SNR without affecting the noise at a given temperature and perform best if they are shaped like a ring and the sample is positioned in the middle of its symmetry axis as it has been theoretically derived with CMT [21]. Hence, DRs are most useful for the applications involving samples with small volume such as small single crystals as proposed by Golovina et al. and Nesmelov et al. [11, 22]. In accordance to Nesmelov et al. [22] and DelMonaco et al. [5] we find an increase of C_i/C_{ref} of about 4 to 5 for the ring-shaped DRs, meaning an enhanced B_1 -field at constant power levels for the coupled DR-cavity system compared to the resonator–cryostat combination alone. In addition, a less thick DR results in higher B_1 -field gains which might be exploited for pulse EPR applications in the future. Our DRs are suited for a large magnetic field and temperature range regarding residual impurities and SNR enhancements with a SNR gain of more than 75 at all temperatures of which a normalized gain of more than 15 is not due to a higher ratio of C_i/C_{ref} but presumably higher filling factors that outreach slightly decreasing quality factors. At temperatures below 77 K we found slightly dropping SNR enhancements which might be due to increasing $\tan \delta$ as seen from Table 1 with the VSWR which shows worse couplings at lower temperatures. Otherwise, from 300 to 6 K the ratio C_i/C_{ref} is constant within the order of errors supporting the high stability on temperature τ_ε reported for the material [24].

The disk-shaped DRs with the sample placed on top have marginal improvements of the SNR due to low field enhancement far from the DR center. It has been shown by Elnaggar et al. [21] that for parallel and antiparallel couplings the magnetic fields at the boundaries of the DR have a minimum which agrees with that result. Furthermore, the dielectric losses increase as the disks contain more of the DR material than the rings. Nevertheless, the major gain in the SNR increase of the disk-shaped DRs is, according to our observations, due to the increase in B_1 -field. In any case, we observe a significant shift of f_{coupled} towards higher coupled resonance frequencies with DRs matched in comparison to the resonator–cryostat combination without DR. This effect agrees well with the observation of Golovina et al. [11] and points towards a $\text{TE}_{01\delta}$ mode coupling antiparallel with the cavity mode. With our DRs we do not observe any other modes within a range of 1 GHz around the observed mode for the given position of the DRs inside the cavity which is presumably far from optimal for an electric coupling, yet the most convenient situation for the application in a flow cryostat.

The full potential of ring DRs is exploited for very small samples with a volume of a portion of a nanolitre (nl) as the DRs allow both for a good positioning of small samples within the hole (orientation maintaining with respect to sample tube) and a signal enhancement of about one order of magnitude and beyond: one advantage of DRs is the fact, that the higher C_i/C_{ref} only leads to stronger mw fields in the vicinity of the sample which has been calculated with CMT [19, 20]. Mett et al. and Elnaggar et al. show that the field conversion constant C which is directly related to the probe's efficiency parameter Λ is crucial for the sensitivity of EPR

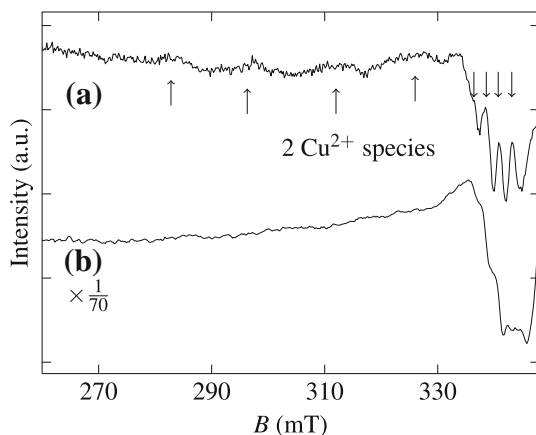


Fig. 5 A twin crystal EPR spectrum of the two Cu^{2+} species with resolved hyperfine splitting in a ${}^3_{\infty}[\{\text{Cu}_2^{\text{I}}\text{Cu}_2^{\text{II}}((\text{Me-trz-mba})_2\text{thio})(\text{H}_2\text{O})_2\}\text{Cl}_2] \cdot 6\text{H}_2\text{O}$ with a volume of 0.01 nl and additionally Cu^{2+} -impurities of the resonator-cryostat combination at 6 K: **a** single scan with K80-H, **b** 70 scans of that crystal with the resonator-cryostat combination where only the Cu^{2+} -impurity of the cryostat is visible

spectrometers. Therefore, the actual SNR increase in comparison with e.g. unwanted impurity signals from the cavity or cryostat may be even higher than the normalized numbers we give in Tables 2, 3, 4 as seen in Fig. 5. Here, the Cu^{2+} EPR spectrum of the single crystal of $\text{Cu-MOF } {}^3_{\infty}[\{\text{Cu}_2^{\text{I}}\text{Cu}_2^{\text{II}}((\text{Me-trz-mba})_2\text{thio})(\text{H}_2\text{O})_2\}\text{Cl}_2] \cdot 6\text{H}_2\text{O}$ is shown to illustrate also this effect. It was recorded under the following conditions: (a) a single-scan spectrum at 6 K and 60 μW using K80-H versus (b) the spectrum of the same crystal recorded in the resonator-cryostat combination alone at 20 times higher mw power to compensate in the later spectrum for $C_i/C_{\text{ref}} = 4.2$. Additionally, 70 scans were accumulated to reduce the noise by a factor of about $\sqrt{70} \approx 8.4$, which is close to the relative SNR enhancement stated in Table 4 for K80-H (8.5). Particularly for the two measurements are the Cu^{2+} impurities in the quartz tube of the cryostat and the inner walls of the cavity. Scaling of the two spectra to compensate for the accumulations shows that these background signals are of the same order of magnitude as expected from the five times higher mw power. However, the typical four line hf EPR spectrum of the Cu^{2+} species from the tiny single crystal is only visible with the DR and not observed in the other measurement using the standard EPR setup. There the mw power increase leads to an increased overall signal while in case of the DR the B_1 field is solely increased in its center where the crystal is positioned. This experiment demonstrates the potential of the application of DRs in particular for studies of tiny single crystal samples. The sample can be kept in thin quartz capillaries for EPR measurements under non-ambient atmospheres in a wide temperature range and an easy transfer to investigations with other methods such as X-ray diffraction analysis is possible.

4 Summary and Conclusion

In summary we present a new series of EPR silent DRs based on barium lanthanide titanates solid solutions (BLTss) with the general formula $\text{Ba}_{6-x}\text{Ln}_{8+2x/3}\text{Ti}_{18}\text{O}_{54}$ ($\text{Ln} = \text{Sm}, \text{Nd}$) with small dielectric losses and dielectric constants of about 80. The developed DRs have shown a good potential in applications as reliable and easy-to-use components. The impurity content is sufficiently low so that baseline signals from the DRs are acceptable. The DRs can easily be used in combination with cavity resonators and flow cryostats for experiments from room temperature down to 6 K. The sample can be kept in quartz-glass tubes for measurements of dehydrated or gas-loaded samples. In principle, disk-shaped DRs can be employed for measurements of thin film samples and ring DRs for low volume samples such as tiny single crystals. The latter perform better at all temperatures with respect to both the relative conversion factors of the mw B_1 -field and normalized SNR gain. We found enhancements of the normalized SNR gain of a factor of up to 19 at room temperature and up to 15 at 6 K and additional B_1 -field enhancements of a factor of about 4.8 at 6 K. We have shown that the latter B_1 -field enhancements must be regarded separately for most cw EPR applications but can be important in case of competing signals from impurities in the resonator–cryostat combination. Then, both the SNR enhancements due to the higher filling factor and the higher B_1 -field solely in the vicinity of the sample readily multiply to a factor of up to 74 at 6 K of enhanced SNR which may save more than the square of that figure in scans compared to measurements without DRs.

Acknowledgments We thank the Deutsche Forschungsgemeinschaft (DFG) for financial support within the priority programs 1362 and 1601. Further our thanks goes out to M. Kobalz and H. Krautscheid of the inorganic chemistry group at Leipzig University for the preparation of the Cu-MOF samples.

References

1. M. Jaworski, A. Sienkiewicz, C.P. Scholes, J. Magn. Reson. **124**, 87 (1997)
2. A. Sienkiewicz, K. Qu, C.P. Scholes, Rev. Sci. Instrum. **65**(1), 68 (1994)
3. G. Lassmann, P.P. Schmidt, W. Lubitz, J. Magn. Reson. **172**, 312 (2005)
4. M.W. Pospieszalski, IEEE Trans. Microwave Theory Technol. MIT **27**(3), 233 (1979)
5. S. del Monaco, J. Brivati, G. Gualtieri, A. Sotgiu, Rev. Sci. Instrum. **66**(10), 5104 (1995)
6. A. Blank, E. Stavitski, H. Levanon, F. Gubaydullin, Rev. Sci. Instrum. **74**(5), 2853 (2003)
7. S.M. Mattar, S.Y. ElNaggar, J. Magn. Reson. **209**, 174 (2011)
8. I.S. Golovina, S.P. Kolesnik, I.N. Geifman, A.G. Belous, Rev. Sci. Instrum. **81**(4), 044702 (2010)
9. A. Sienkiewicz, B. Vilen, S. Garaj, M. Jaworski, L. Forro, J. Magn. Reson. **177**(2), 261 (2005)
10. S.M. Mattar, A.H. Emwas, Chem. Phys. Lett. **368**, 724 (2003)
11. I. Golovina, I. Geifman, A. Belous, J. Magn. Reson. **195**, 52 (2008)
12. I. Geifman, I. Golovina, V. Kofman, E. Zusmanov, Ferroelectrics **234**(1), 81 (1999)
13. I. Geifman, I. Golovina, Concepts Magn. Reson. **26B**(1), 46 (2005)
14. H.R. Yi, N. Klein, IEEE Trans. Appl. Superconductivity **11**(1), 489 (2001)
15. A. Blank, E. Suhovoy, R. Halevy, L. Shtirberg, W. Harheit, Phys. Chem. Chem. Phys. **11**(31), 6689 (2009)
16. A.A. Kishk, Y.M.M. Antar, in *Antenna Engineering Handbook*, ed. by J.L. Volakis (McGraw-Hill, New York, 2007), chap. 17

17. D. Kajfez, P. Guillon (eds.), *Dielectric Resonators* (Artech House, Dedham, MA, 1986)
18. Oxford Instruments, Cryostats for Electron Spin Resonance Spectroscopy. <http://www.oxford-instruments.com>, DF OI64802104 (2004).
19. R.R. Mett, J.W. Sidabras, I.S. Golovina, J.S. Hyde, *Rev. Sci. Instrum.* **79**(9) (2008).
20. S.Y. Elnaggar, R. Tervo, S.M. Mattar, *J. Magn. Reson.* **245**, 50 (2014)
21. S.Y. Elnaggar, R. Tervo, S.M. Mattar, *J. Magn. Reson.* **238**, 1 (2014)
22. Y.E. Nesmelov, J.T. Surek, D.D. Thomas, *J. Magn. Reson.* **153**, 7 (2001)
23. C.P. Poole Jr, *Electron Spin Resonance* (Interscience Publishers, New York, 1967)
24. A. Belous, O. Ovchar, M. Valant, D. Suvorov, *J. Appl. Phys.* **92**(7), 3917 (2002)
25. J.E. Wertz, P. Auzins, *Phys. Rev.* **106**, 484 (1957)
26. J. Lincke, D. Lässig, M. Kobalz, J. Bergmann, M. Handke, J. Möllmer, M. Lange, C. Roth, A. Möller, R. Staudt, H. Krautscheid, *Inorg. Chem.* **51**(14), 7579 (2012)
27. R. Fricke, H.G. Jerschkewitz, G. Öhlmann, *J. Chem. Soc. Faraday Trans. 1 Phys. Chem. Condensed Phases* **82**(11), 3479 (1986).